

Defect Control in Zr-Based Metal–Organic Framework Nanoparticles for Arsenic Removal from Water

Nisrine Assaad, Ghewa Sabeh, and Mohamad Hmadeh*



Cite This: *ACS Appl. Nano Mater.* 2020, 3, 8997–9008



Read Online

ACCESS |



Metrics & More



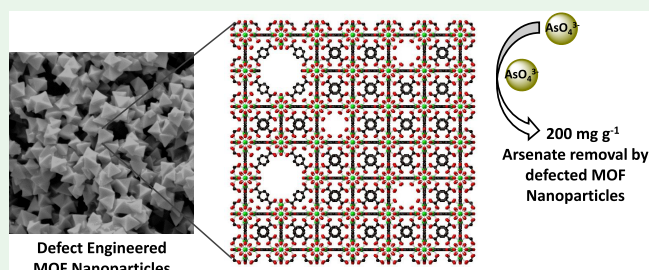
Article Recommendations



Supporting Information

ABSTRACT: In this study, water-stable Zr-metal–organic framework (MOF) (UiO-66) nanoparticles of various defect concentrations were successfully prepared and examined as the adsorbent for arsenate removal from water. The induced defects resulted from the addition of a monocarboxylic acid modulator [acetic acid or trifluoroacetic acid (TFA)] to the synthesis mixture. The concentrations of the defects were effectively tuned and controlled by changing the type and the amount of the modulator. As a result, different adsorption capacities for arsenate from water were obtained, in which the most modulated sample (UiO-66-36TFA) which was obtained by using TFA as the modulator showed an adsorption capacity around 200 mg g^{-1} at neutral pH that is the highest not only among the studied samples but also, up to our knowledge, among all other reported MOFs at neutral pH. By introducing the defects in UiO-66, the arsenate uptake percentage was enhanced by more than 100% compared to defect-free UiO-66 tested in this study. The superior arsenic uptake is attributed to the free Lewis acid sites formed in the MOF clusters as a result of missing linker defects. In addition, the nanoparticles showed outstanding arsenate selectivity against interfering anions and were efficiently recycled to maintain the same adsorption capacity after five regeneration cycles. Furthermore, a small quantity of this sample (0.5 mg) was employed to completely remove ultratrace arsenate (5 ppb), proving its high efficiency in real-life applications. Accordingly, defected nanoscale UiO-66 samples pave the way for future water purification technologies.

KEYWORDS: arsenic, metal–organic frameworks, defects, water, modulator



1. INTRODUCTION

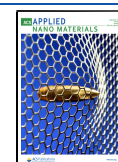
Environmental pollution has attracted the global interest for becoming a scaring issue threatening the entire biosphere.¹ One of the most hazardous contaminants presented widely in water and affecting the environment is arsenic because of its enormous toxicity and carcinogenicity even at low concentrations.² Short-term exposure to high concentration of arsenic proved to result in skin lesions, hyperkeratosis, and cancer of internal organs.³ Therefore, World Health Organization (WHO) and the Environmental Protection Agency (EPA) classified arsenic as the first priority contaminant among the hazardous substances and declared that the limit of arsenic concentration for the drinking water is less than 10 ppb.⁴ However, arsenic levels exceed this limit in contaminated ground water and industrial waste water where the arsenic ranges between 0.5 and 3 ppm and is higher than 100 ppm, respectively.⁵ Accordingly, several technologies have been developed to eliminate arsenic from drinking water including reverse osmosis, chemical coagulation, membrane filtration, ion-exchange, and adsorption methods.⁶ Because of its robust usage, high efficiency, and cost effectiveness, adsorption proved to be one of the most promising efficient remediation techniques for As removal.⁷ A wide range of adsorbents have been reported in the literature for arsenic removal. This

includes boehmite, alumina, activated carbon, hydrated ferric oxide, activated alumina, iron- and manganese-coated sand,^{8–12} fly ash, clays, chitosan resins, and cation-exchange resins in addition to other natural and synthetic materials.^{13–16} However, most of the established adsorbents have many limitations such as unsatisfactory capture capacity (less than 100 mg g^{-1}), slow kinetics, and poor selectivity increasing the need for new efficient adsorbents. Recently, a new class of porous materials is being explored for toxic elements adsorption and it is expressed by metal–organic frameworks (MOFs).¹⁷ MOFs are porous crystalline solids composed of inorganic metal clusters connected to organic linkers via strong coordination bonds and arranged in extended networks.^{18,19} Because of their unprecedented characteristics such as ultrahigh internal surface area, abundant exposed metal sites, adjustable pore sizes, easily tunable properties, and great mechanical and thermal stability,^{20–22} MOFs grabbed the attention in the field

Received: June 22, 2020

Accepted: August 14, 2020

Published: August 14, 2020



of material chemistry and are widely used in enormous applications including gas storage, catalysis, drug loading, magnetism, conductivity, biochemical imaging, selective separation, and adsorption.^{23–27} Despite the current progress, most of the MOFs reported cannot be applied in water treatment because they are pH-sensitive and thus nonstable in water.²⁸ Some of the chemically stable MOF structures have been used in adsorption for the aim of removing toxic elements from water such as ZIF-8,²⁹ AUBM-1,³⁰ Zn-MOF-74,³¹ MIL-53,³² and UiO-66.³³ However, among the mentioned MOF materials, UiO-66 showed the highest arsenic uptake capacity by comparison with other commercial and synthetic adsorbents.³³

The UiO-66 structure consisting of octahedral $Zr_6O_4(OH)_4$ clusters linked to 12 terephthalate (1,4-benzenedicarboxylate, BDC) bridging ligands is the most used MOF adsorbent for pollutant removal (organic and inorganic) from water because of its interesting properties, involving low toxicity, ecofriendly nature, and high water and chemical stability.³⁴ In this particular case of arsenate adsorption on UiO-66, it is mainly due to Lewis acid–base interactions between Zr–OH groups of the MOF and arsenate. The acidity of the MOF is controlled by many factors including the formation of defects in their structure providing additional and accessible Lewis acid sites on the Zr cluster.^{35,36} It has been demonstrated that the addition of monocarboxylic acid “modulators” to the synthesis mixture enhances the production of defects,^{37,38} which in general affect positively the reactivity,³⁹ stability,⁴⁰ porosity,⁴¹ thermomechanical behavior,⁴² and adsorption capacities⁴³ of the defected MOF structures. Following this strategy, two kinds of defects can be produced in the UiO-66 framework: “missing-linker defect” and “missing-cluster defect”.^{36,44} The missing linker defect that was discovered by the Zhou group⁴³ was the result of acetic acid (AA) addition to the synthesis mixture. By acting as the defect-compensating ligand, AA boosts the creation of this defect in a directly proportional way leaving behind two neighboring metal clusters with coordination-free sites acting as Lewis acid sites.⁴⁵ Vermoortele et al. had similar observations by making intensely defective UiO-66 samples via trifluoroacetic acid (TFA) as a modulator.⁴⁶ On the other hand, Goodwin and his co-workers discovered that using formic acid as a modulator induces the formation of missing cluster defect that occurs in the correlated nanoregions of the reo topology of UiO-66.⁴⁷ As a result, the clusters will have lowered linker affinity in the defective reo phase⁴⁸ and imbalance in the charge which is compensated by formate ions. In other words, missing-cluster defect is the case of cluster deletion with its coordinated 12 linkers and the insertion of one coordination vacancy on the adjacent cluster.⁴⁹ In addition, the magnitude and thus the effect of the defect can be tuned by varying the amount of the modulator or even the type of the modulator (different modulators of different acidities).⁴⁴ Both defects have the same influence of having free active sites ready for coordination, adsorption, catalysis, and many other applications.⁵⁰ Furthermore, to shed light on the importance and effect of these defects, it was reported that the properties of the MOFs are directly related to the role of metal clusters⁵¹ and in specific to the coordination vacancies caused by the mentioned defects.^{35,52} Recent studies have focused on the action of defected MOFs in water decontamination from toxic elements⁵² such as selenites,^{53,54} phosphates,⁵⁵ and mercury⁵⁶ in addition to gas separation^{43,57} and dye adsorption.⁵⁸

However, to the best of our knowledge, only one study on investigating the effect of the defects on the performance of UiO-66 on the arsenate removal from water has been done so far.⁵² Herein, we show how the introduction of defects on the MOF cluster greatly improves the As uptake by UiO-66, which has been reported to be the best As adsorbent MOF material.³³ To this end, two types of modulators (AA and TFA) and their effects on the structural properties of the obtained MOF nanoparticles were investigated and compared with the ideal nonmodulated UiO-66 MOF. Six samples were synthesized by the solvothermal procedure and fully characterized by scanning electron microscopy (SEM), powder X-ray diffraction (PXRD), Brunauer–Emmett–Teller surface area analyzer (BET), Fourier-transform infrared spectroscopy (FT-IR), and thermogravimetric analysis (TGA). Their performance as adsorbents for arsenate removal from water was studied, and the thermodynamic and kinetic parameters of the adsorption process were determined, and the obtained results were compared with the nonmodulated UiO-66 structure. The relationship between the concentration of the sample’s defect from one side and arsenate removal efficiency from the other side was also discussed, and great insights into the properties and the nature of the defect in the samples and the adsorption extent of each modulated MOF were obtained. Our approach of introducing defects in UiO-66 appears to be very efficient for arsenic removal and an enhancement of more than 100% was obtained with the defected MOFs when compared to the defect-free UiO-66 tested in this study. More importantly, ultratrace arsenic was removed efficiently by the best member (UiO-66-36TFA) of our defected UiO-66 series, proving the excellent performance of these modulated samples in water treatment process and opening the gate for advanced vision of MOFs in arsenic removal industry.

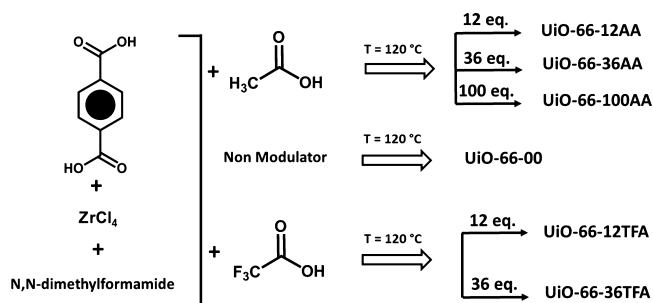
2. MATERIALS AND METHODS

2.1. Materials. All chemicals needed for the study were purchased and used directly as received. Zirconium chloride ($ZrCl_4$, 98%) and terephthalic acid [$C_6H_4(CO_2H)_2$, 99%] were obtained from Acros Organics. Acetic acid glacial ($C_2H_4O_2$, 99%) and TFA were obtained from Fisher Scientific. Sodium arsenate dibasic heptahydrate, *N,N*-dimethylformamide (DMF, analytical reagent grade), dichloromethane (DCM, analytical reagent grade), sodium nitrate, sodium carbonate, sodium sulfate, sodium bicarbonate, sodium chloride, sodium formate, and sodium acetate were obtained from Sigma-Aldrich.

2.2. Synthesis of the Adsorbents. UiO-66 samples were synthesized under conditions similar to those reported in the literature with slight modifications by changing the ratio of AA and TFA.⁵³ Briefly, $ZrCl_4$ (1.724 g, 7.398 mmol) and terephthalic acid (1.230 g, 7.402 mmol) were dissolved in DMF (200 mL, 2582 mmol) by sonication for 10 min at room temperature. Following so, deionized water (0.4 mL, 22.2 mmol) and different ratios of modulators (details in Table S1 and Scheme 1) were added to the mixture that was in a 500 mL autoclavable reagent bottle and put in a preheated oven at 120 °C for 3 days. The obtained microcrystalline powders were collected from the solutions by centrifugation and washed with 55 mL of DMF three times separated by 3 h’ time interval, soaked overnight in the solution, and then washed three times with DCM for 3 days. After the washing procedure, the collected precipitate was dried in a vacuum oven at 100 °C overnight.

2.3. Characterization of the Adsorbents. The six samples were fully characterized by SEM–energy-dispersive X-ray spectrometry (SEM–EDX), PXRD, BET surface area analyzer, FT-IR, and TGA. N_2 adsorption–desorption isotherms were measured using a Quantachrome-NOVA 2200e-surface area and pore size analyzer that provided significant information concerning the effect of defect

Scheme 1. Schematic Presentation of the Synthesis Conditions of the Six MOF Samples in This Study



on the MOF. The P/P_0 range where the BET equation was fitted was between 0.07249 and 0.99187 and the P/P_0 value at which the pore volume was measured was 0.991. SEM imaging was done using a MIRA3 TESCAN electron microscope after coating the samples with a thin layer (20 nm) of platinum. TGA was performed with a NETZSCH TG 209 F1 Libra apparatus under a N_2 /air flow from 30 to 1095 °C at a heating rate of 3 K min^{-1} . PXRD patterns of the MOF samples were recorded with a Bruker D8 ADVANCE X-ray diffractometer (Bruker AXS GmbH, Karlsruhe, Germany, working at 40 kV and current 40 mA, 2θ range: 6–50°, increment: 0.02°) using Cu $K\alpha$ radiation ($k = 1.5418 \text{ \AA}$). The infrared spectra were collected on a FT-IR spectrometer Thermo-Nicolet in the transmittance mode, in the 450–3950 cm^{-1} range. Arsenic concentration was calculated using atomic absorption spectroscopy (AAS) conducted with a thermo elemental analyzer.

2.4. Arsenate Adsorption Experiments. Several parameters were changed for the sake of studying the effect of different experimental conditions on the arsenate removal efficiency. The varying parameters ranged among pH, concentrations, contact time, and temperature. The arsenic solutions used were prepared by dissolving the appropriate mass of sodium arsenate dibasic heptahydrate in a certain volume of deionized water. All arsenic adsorption experiments were done at room temperature except for that involving temperature effect. For the pH, temperature, and time effect experiments, 10 mL volume of the arsenate solution with an As (V) initial concentration of 100 $mg L^{-1}$ and 10 mg of activated UiO-66 MOF (six different samples) adsorbents were placed in Falcon tubes shaken at the rate of 200 rpm for 3 h.

First of all, kinetic study was done to determine the time of maximum adsorption where each tube was removed from the shaker at the allocated time from 2 min to 72 h. The concentration of As (V) in the solution drops down till it reaches equilibrium after 3 h. For the pH effect experiment, each tube had a specified pH which ranged between 2 and 10. The exact pH values were controlled via 1 M hydrochloric acid and 2 M sodium hydroxide solutions. However, for

the temperature effect, every Falcon tube was placed at different temperatures between 25 and 55 °C with 10 °C increment.

To examine the effect of arsenic concentration [As (V)] on the adsorption capacities, 10 mL of arsenate solutions of different concentrations ranging from 10 to 300 $mg L^{-1}$ (pH = 7.6) and 10 mg of activated UiO-66 MOF (six different samples) were mixed in each tube. At the end of each experiment, the supernatant was filtered through a 0.20 μm filter and the remaining arsenic concentrations of the filtrates were measured using AAS.

The equilibrium adsorption capacity q_e ($mg g^{-1}$) was calculated using eq 1

$$q_e = \frac{C_0 - C_e}{m} V \quad (1)$$

where C_0 is the initial concentration of arsenate (in $mg L^{-1}$), C_e represents the concentration of arsenate at equilibrium (in $mg L^{-1}$), m is the mass of the MOF (in g), and V is the volume of the solution (in L).

2.5. Arsenic Adsorption in the Presence of Anions. In studying the effect of anions on arsenic adsorption, UiO-66-36TFA MOF that showed the highest adsorption capacity was chosen to be worked on. In brief, seven falcon tubes (15 mL capacity) were used each containing 10 mg of the activated MOF, 10 mL of 60 ppm arsenic solution, and 10 mM of one of the following anions: $NaNO_3$, Na_2CO_3 , Na_2SO_4 , $NaHCO_3$, CH_3COONa , $HCOONa$, $NaCl$, and Na_3PO_4 . After 12 h of shaking at 25 °C, the solution was filtered and the remaining arsenic concentration was determined using AAS.

2.6. Arsenic Recovery. Methanol (10 mL) was added to 30 mg of the As-loaded MOF and was constantly shaken for 12 h. Then, the recycled samples were dried out and 30 mg was tested with 10 mL of arsenic solution of 150 ppm initial concentration. This process was repeated five times for the same sample.

2.7. Proton NMR Measurement. Nuclear magnetic resonance (NMR) digestion was based on a previously reported method using sodium bicarbonate ($NaHCO_3$). $NaHCO_3$ (10 mg) was dissolved in $DMSO-d_6$. The solution has been sonicated and then added to 5 mg of UiO-66 samples, which was further sonicated and transferred to an NMR tube.

3. RESULTS AND DISCUSSION

3.1. Characterization. The experimental PXRD patterns of the six nanoscale MOFs shown in Figure 1A are identical, revealing sharp narrow peaks and matching perfectly with the reported one in the literature⁵³ without any additional peaks, confirming the high phase purity and crystallinity of the MOF samples. It is noteworthy to mention that the PXRD pattern of UiO-66-36TFA represented in Figure S1A showed the presence of an extra broad peak at 3.8°, which is believed to correspond to the ordered missing cluster defects in the UiO-66 structure.⁴⁴ The proposed defect is related to the reflected

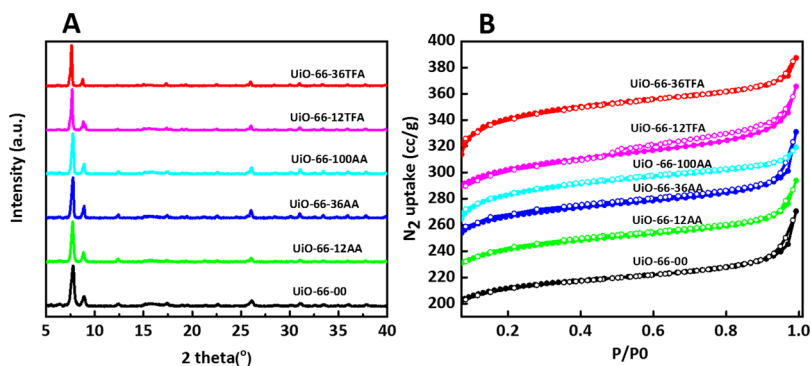


Figure 1. (A) XRD analysis of the UiO-66 samples. (B) N_2 adsorption–desorption isotherms of the UiO-66 samples, adsorption (filled circles); desorption (empty circles).

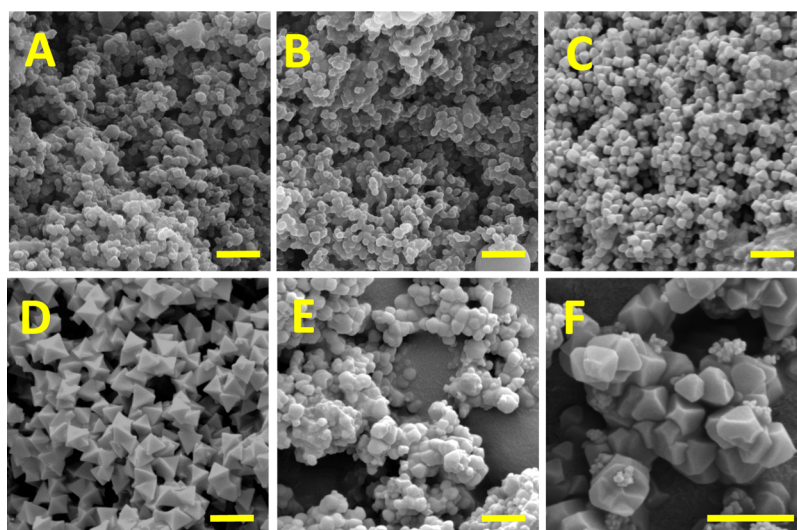


Figure 2. SEM images of the studied MOF nanoparticles (A) (UiO-66), (B) (UiO-66-12AA), (C) (UiO-66-36AA), (D) (UiO-66-100AA), (E) (UiO-66-12TFA), (F) (UiO-66-36TFA) with a 1 μm scale bar.

Bragg peak from (100) plane of the missing cluster defect because of the 3-periodic 8-connected reo net.⁵⁹ Moreover, pore size distribution graphs for UiO-66-00 and UiO-66-36TFA are shown in Figure S1B, where the appearance of new peaks between 15 and 20 Å is observed for UiO-66-36TFA that is due to missing cluster defects in the mentioned sample.⁶⁰

To evaluate the surface area and the porosity of the synthesized MOFs, textural properties were examined by the N₂ adsorption–desorption technique at 77 K. The obtained isotherms are exposed in Figure 1B, whereas the resulted BET surface areas and pore volumes are summarized in Table S1. All of the MOF samples had similar type-I behaviors that are in good agreement with the reported observations in the literature.⁵³

Depending on the type of modulator and its ratio, the resulting surface area and porosity vary between the different nanoparticles. As expected, the surface area and porosity were the lowest for the sample synthesized without any modulator, and they increased as the amount of the modulator increased from one side and as the acidity of the modulator increased ($\text{p}K_{\text{a}}$ decreased) from another side in a way that they were higher for the samples modulated with TFA than with AA. These two factors showed the important extent to which the characteristics of UiO-66 can be tuned by the addition of an acidic modulator. Quantitatively, the BET surface areas of the MOF samples differed considerably, ranging from 1041 $\text{m}^2 \text{g}^{-1}$ (without any modulator) to 1690 $\text{m}^2 \text{g}^{-1}$ (with TFA) and increasing in the trend mentioned above.

The morphology of the nanocrystals was investigated by high-resolution SEM and representative images are depicted in Figure 2. The obtained micrographs show uniform octahedral shaped crystals of the samples of high modulator concentrations (above 12 equiv), indicating their homogeneity and high purity. The average particle size of each sample was calculated through SEM images, and the values are represented in Table S1. Typically, adding 88.8 mmol of AA (UiO-66-12AA) resulted in irregular, aggregated, and smaller crystals with the size of 112 nm and it increased with the increase in the amount of added AA. However, adding the same number of moles of TFA gave relatively larger crystals of size 120 nm

and this size also elevated with the increase in the TFA amount to give a well-defined octahedral shape for UiO-66-35TFA.

TGA was used to reveal the structural “imperfections” of the studied MOFs by calculating the number of missing linkers in each sample according to the method reported previously in the literature.⁴⁴ The TGA curves for the six MOFs presented in Figure S2 are normalized, and W_{end} , the end weight of the TGA run, is taken to be 100%. W_{theo} represents the theoretical weight loss plateau, W_{exp} is the experimental weight loss plateau, and Temp pl is the temperature at which the plateau (W_{exp}) is reached.

By examining the six TGA curves, three weight losses could be observed in each one; the first weight loss is due to the removal of the adsorbed H₂O, and it occurs in the range of 35–100 °C, which is a common temperature range for all the MOFs. The second step is the dehydroxylation of the zirconium cluster and elimination of the monocarboxylate linkers,^{46,61} and it extends from 100 °C till temperature plateau (Temp pl), that is specific for each MOF. Temp pl is the temperature of the combustion of the linker and it marks the beginning of the third step which is the framework destruction phase. Because Temp pl is unique for each MOF, the temperature range for the third step is different for each one. By analyzing Figure S2, the third weight decrease step of UiO-66-00 and UiO-66-36AA starts from 390 °C, whereas it was found to be 350 °C for UiO-66-12AA and 450 °C for the remaining three samples (UiO-66-100AA, UiO-66-12TFA, and UiO-66-36TFA). TGA is considered an effective tool in investigating quantitatively the defects present in the MOFs.^{44,62} The theory behind this is the fact that the number of missing linkers found in a structure is inversely proportional to the weight loss plateau related to linker combustion.^{40,63} That is, the higher the number of missing linkers, the lower the percentage of the linker mass relative to the total mass of the structure and thus the smaller the related weight loss plateau observed. The gaps between the line representing W_{theo} and the one representing W_{end} and that between W_{exp} and W_{end} indicate, respectively, the theoretical and experimental weight losses attributed to the linker combustion. It could be noticed that the theoretical weight loss is greater than the experimental one, assuring the fact that the samples are linker deficient. The

number of missing linkers was than calculated for all samples, and the obtained values are included in Table S1.

To further characterize the defected samples, proton NMR was done for UiO-66-36TFA, UiO-66-100AA, and UiO-66-00, as represented in Figure S3. Besides the solvent peak at 2.5 ppm, the NMR showed the presence of one peak (of chemical shift = 8 ppm for UiO-66-36TFA, 7.5 ppm for UiO-66-100AA, and 7 ppm for UiO-66-00) that refers to the identical hydrogens of the aromatic ring of terephthalic acid that assures the absence of any other hydrogens coming from any remaining acid modulator. Thus, no residual monocarboxylic acid modulators are found in the three samples.

4. AS ADSORPTION STUDY

4.1. pH Effect. After the synthesis and full characterization of the six nanoscale UiO-66 MOF samples, their ability to be employed as adsorbents for arsenate removal from water was investigated. Taking into consideration the enormous effect of solution pH in the process of adsorption, as it influences not only the structure and surface charge of the adsorbent but also the various species of arsenate ions involved, several experimental batches were conducted to study the pH effect and thus to identify the optimal pH of arsenate adsorption.

Arsonate is pH-dependent, for example, at pH below 2.1, the predominating form is H_3AsO_4 , and as pH increases from 2.1 to 6.7, H_2AsO_4^- becomes predominant. Finally, when the pH becomes greater than 6.7, the HAsO_4^{2-} species invade.³³

Getting into the details of the experiment, the MOFs were dispersed in arsenate solutions of pH values between 2 and 10 and the results are shown in Figure 3. As shown in the figure,

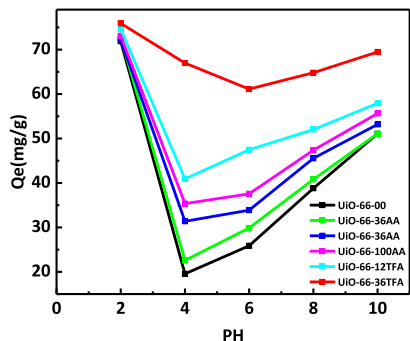


Figure 3. Adsorption of As at different pH values $C_0 = 100 \text{ mg L}^{-1}$, $V = 10 \text{ mL}$, $m = 10 \text{ mg}$, and $t = 3 \text{ h}$.

all of the MOFs except for UiO-66-36TFA followed the same trend; the highest removal efficiency was at acidic conditions (pH = 2) and then it dropped down to the minimum as pH increased to 4, to 7 to finally increase as pH increased to 10. On the other hand, UiO-66-36TFA showed approximately the same behavior among all pHs (decrease of 15%), indicating its stability and its independency on solution pH in the adsorption process.

In order to study the surface charges of the different samples, zeta potential was measured for UiO-66 and UiO-66-36TFA and the data are shown in Figure S4. Both MOFs showed the same zero-point charge at pH = 4.3, which implies the positive charge of the adsorbents' surfaces below this pH and their negative charge above it. By comparing these data and that of arsenic predominant species at each pH, it could be concluded that electrostatic attraction played a certain role in this mechanism; for example, starting from 2.2 to 4.3 pH range, the uptake was high because the negatively charged arsenate was strongly attached to the positively charged surfaces of the MOF samples and decreased to the minimum at the zero-point charge (pH = 4.5) because of the neutrality of the adsorbent surface. At pH = 2, the arsenate is in its neutral form (H_3AsO_4), so the adsorption was expected to be very low because of the absence of charge; however, it was noticed that the highest uptake was at this pH, indicating that electrostatic interaction was not the only controlling factor in the process. Arsenate ions attach to the MOF via two coordination processes that are similar to acid–base interactions in a way that very acidic conditions favor the release of H^+ from H_3AsO_4 and thus increase its binding to the hydroxyl sites in the sample.³³ Following this, arsenate uptake started to increase with the increase in pH (4–10 range), which is due to acid base interactions between the acidic MOF and basic arsenate (H_2AsO_4^- and HAsO_4^{2-}). From the obtained graph, it can be seen that the removal efficiency increased as the defect increased [the ratio of the modulator was greater or the acidity of it was higher (lower $\text{p}K_a$)]; in other words, the removal capacity was the lowest for UiO-66 having no added modulator, and it increased as AA concentration increased ($\text{UiO-66-12AA} < \text{UiO-66-36AA} < \text{UiO-66-100AA}$). It is noteworthy to mention that the arsenate uptake for the highest defected sample (UiO-66-36TFA) was not that much affected by the pH change as the other samples. Furthermore, all AA-modulated MOFs showed lower adsorption ability than those modulated with TFA and the highest efficiency was recorded for UiO-66-36TFA of the highest defect. Despite all

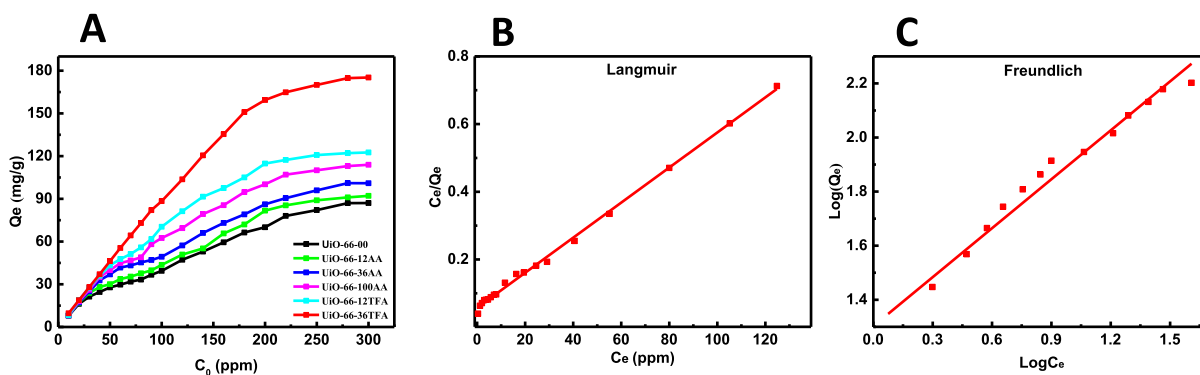


Figure 4. (A) Arsenate removal by modulated MOFs at different concentrations ($10 \text{ mg L}^{-1} \leq [\text{As}] \leq 300 \text{ mg L}^{-1}$) from water and (B) data fitting using Langmuir and (C) Freundlich models for UiO-66-36TFA.

Table 1. Thermodynamic Parameters of Arsenate Adsorption over the Synthesized Samples at Different Temperatures

	ΔH° (kJ mol ⁻¹)	ΔS° (J mol ⁻¹ k ⁻¹)	ΔG° (kJ mol ⁻¹)			
			298 K	308 K	318 K	328 K
UiO-66-00	17.85	54.79	1.52	0.97	0.43	-0.12
UiO-66-12AA	19.12	60.93	0.96	0.35	-0.25	-0.87
UiO-66-36AA	19.56	62.59	0.91	0.29	-0.34	-0.97
UiO-66-100AA	18.04	59.07	0.43	-0.16	-0.75	-1.34
UiO-66-12TFA	16.66	55.94	-0.01	-0.57	-1.13	-1.69
UiO-66-36TFA	14.06	50.06	-0.86	-1.36	-1.86	-2.36

of this and for practical reasons, all the thermodynamic and kinetic studies will be performed at neutral pH.

4.2. Concentration Effect. The arsenate adsorption isotherms on the six MOF samples were performed over various concentrations of arsenic solution ranging from 10 to 300 ppm. In the six samples, the adsorption capacity increased as the concentration increased until it reached the saturation at 280 ppm. This attitude is justified by the fact that higher concentration gradient means larger mass transfer (more driving force). In addition, it provides more available arsenic ions in the vicinity of the active sites on the surface of the MOF, thus increasing the probability of surface adsorption. Concerning the variation in the adsorption capacities, it was noticed that also here the capacity increased as the defect increased. The collected data were investigated by Langmuir (eq 2) and Freundlich (eq 3) models and plotted in Figure 4B,C for UiO-66-36TFA and in Figures S5–S7, for the remaining samples, whereas the parameters of the best fits are shown in Table S2.

$$\frac{C_e}{q_e} = \frac{C_e}{q_{\max}} + \frac{1}{K_L q_{\max}} \quad (2)$$

$$\log q_e = \log K_F + \frac{1}{n} \log C_e \quad (3)$$

where q_e (mg g⁻¹) is the adsorbed quantity at equilibrium, C_e (mg g⁻¹) is the concentration at equilibrium, q_{\max} represents the maximum adsorption capacity, K_L (L mg⁻¹) is an equilibrium constant linked to the binding strength, n and K_F (L mg⁻¹) are Freundlich constants that express the adsorption capacity and adsorption intensity, respectively.

The highest correlation coefficient (R^2) determines the type of isotherm; in the six samples, Langmuir model had the greater R^2 indicating a monolayer process (Figures S5–S7). Surprisingly, UiO-66-36TFA had the highest uptake not only among the six tested samples (200 mg g⁻¹) but also among all reported MOFs at neutral pH and most of the commercial and synthetic adsorbents, as summarized in Table S3.

This proved the importance of defect control in the adsorption process, making defected UiO-66 samples a great prospective for water treatment.

4.3. Temperature Effect. Temperature is a crucial factor to be studied in the process of wastewater treatment, keeping in mind the fact that polluted water is released by industry over different temperatures. Figure S8 represents the effect of temperature on arsenic adsorption experiments.

Two trends were observed, the first one is represented by the increase in the adsorption capacity as the temperature increased, where the highest capacity was for UiO-66-36TFA and increased from 58 to 70 mg g⁻¹ as temperature increased from 25 to 55 °C. However, the second trend showed high

capacities with increasing the MOF defect (increasing modulator acidity or modulator ratio).

In studying the thermodynamics of the reaction, van't Hoff equation (eq 4)⁶⁴ was used to calculate the adsorption enthalpy (ΔH°) and entropy (ΔS°)

$$\ln K_L = \frac{\Delta S^\circ}{R} - \frac{\Delta H^\circ}{RT} \quad (4)$$

where K_L is the equilibrium constant calculated using the formula $K_L = q_e/C_e$ (L g⁻¹). By plotting $\ln K$ versus $1/T$, as shown in Figure S9, the enthalpy and the entropy of the various MOF samples are illustrated in Table 1.

After calculating the values of entropy and enthalpy, Gibbs free energy was calculated from eq 5 and the results are represented in Table 1.

$$\Delta G^\circ = \Delta H^\circ - T\Delta S^\circ \quad (5)$$

For all samples studied, the changes in enthalpy (ΔH_{ads}) are calculated to be positive and within the same range (14.06 and 19.56). Because of their positive values of all the samples, it can be deduced that the process of arsenate removal is an endothermic process, taking place on the surface of the samples (mostly physisorption on the surface), and due to strong interaction forces between the arsenate anions and the Lewis acid sites or the Brønsted acid sites created by the defects on the frameworks as fully developed in the introduction.

Concerning ΔS° , its positive value (ranging from 54.79 to 62.59) shed light on the randomness of solid/solution interface and on the increase in the degree of freedom of the arsenate being adsorbed.

Finally, concerning the values of ΔG° , the results were interesting. All ΔG° for the defected samples were negative at high temperatures (318 and 328 K) and started to decrease as the defects increase, indicating the spontaneity of the adsorption of the adsorption process and the importance of defect in making the reaction spontaneous for enhanced arsenic adsorption. It can be observed that some of the values are positive at low temperatures, but these numbers are very close to zero which is the boundary, meaning that this could be due to experimental errors, in a way that even at low temperatures, the nonspontaneous character is not recognizable and does not contradict with the spontaneity of the studied adsorption reaction. This is explained by the fact that more defected samples have more exposed open metal sites for the arsenate ions to be attached on. However, at low temperatures (298 and 308 K), ΔG° values were positive for the samples made with AA and negative for those made with TFA. This implies the spontaneity of adsorption for the most defected samples (made with TFA) even at low temperatures and the nonspontaneity of the less defected ones at low

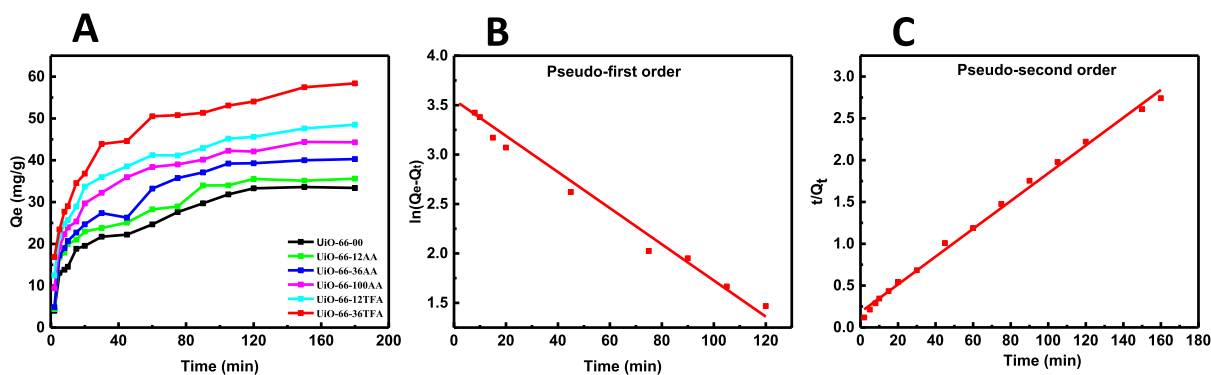


Figure 5. (A) Arsenate uptake as a function of contact time, (B) pseudo-first-order fit for UiO-66-36TFA, (C) pseudo-second-order fit for UiO-66-36TFA. $C_0 = 100 \text{ mg L}^{-1}$, $V = 10 \text{ mL}$, $m = 10 \text{ mg}$ and $T = 25 \text{ }^\circ\text{C}$.

temperatures, which was expected because ΔG° is temperature-dependent.

4.4. Kinetic Study. In order to investigate the mechanistic aspects of the arsenate adsorption, practical understanding of the arsenate adsorption kinetics on the various defected UiO-66 samples must be acquired and the equilibrium of the adsorption process must be determined. To study the adsorption rate of the adsorbents with increasing defect toward arsenate, the arsenate uptake as function of the contact time was studied and the obtained results are shown in Figure 5A. With time, the remaining arsenate concentration declined until it reached equilibrium. By analyzing the kinetic curves, it could be noticed that the adsorption was fast at the beginning when the concentration gradient was high and slowed down as time passed by. It can be also clearly seen that higher and faster adsorption was observed for the highly defected sample which can be explained by the fact that more adsorption sites are available in the UiO-66-36TFA structure. To explore deeply the mechanism of adsorption, pseudo-first-order (eq 6)⁶⁵ and pseudo-second-order (eq 7)⁶⁶ kinetic models are used to extract the kinetic parameters of the adsorption process. Briefly, the pseudo-first-order model proposes that the rate of variation in the solute concentration with time and the variation in the adsorbent concentration in addition to the quantity of adsorbate over time are logarithmically proportional. However, the pseudo-second-order model suggests that the adsorption capacity of the adsorbent is directly proportional to the number of active sites occupied on it.

$$\ln(q_e - q_t) = \ln q_e - k_1 t \quad (6)$$

$$\frac{t}{q_t} = \frac{1}{k_2 q_e^2} + \frac{t}{q_e} \quad (7)$$

where q_e (mg g^{-1}) is the equilibrium adsorption capacity found experimentally, q_t (mg g^{-1}) is the adsorption quantity at time t , and k_1 (min^{-1}) and k_2 ($\text{g mg}^{-1} \text{min}^{-1}$) are the pseudo-first-order and pseudo-second-order rate constants, respectively.

The fitted data for UiO-66-36TFA are given in Figure 5B,C, whereas for the remaining MOFs, data fits are shown in Figures S10–S12. The resulted parameters are summarized in Table S4.

For all of the MOF samples, the correlation coefficients (R^2) of the pseudo-second-order model had greater value than pseudo-first-order, and the calculated equilibrium capacity q_e was found to be in good agreement with the experimental one. The obtained results indicate that the kinetics of adsorption

followed the pseudo-second-order model. This implies that the chemisorption process is forceful, and the arsenates are greatly adsorbed on the surface.

It is noteworthy to mention that adsorption mechanism is both physisorption (positive enthalpy) and chemisorption (kinetics of adsorption followed the pseudo-second-order model) at the same time keeping in mind that these cases are rare but happen to occur.^{31,67}

For better analysis of the overall rate of the adsorption process, an intraparticle diffusion model⁶⁸ was developed through eq 8

$$q_t = k_{id} \cdot t^{1/2} + \theta \quad (8)$$

where k_{id} represents intraparticle diffusion rate constant [$\text{mg} (\text{g min}^{1/2})^{-1}$], and θ is a constant linked to the thickness of the boundary layer (mg g^{-1}) which increases with θ . The plots of q_t against $t^{1/2}$ for all samples are displayed in Figure S13 and show that the rates of adsorption are obviously a three step-controlled process (multistage controlled). The adsorption process starts with the diffusion of arsenate to the surface of the MOF (external surface adsorption) followed by the progressive adsorption of arsenic ions in the samples (intraparticle diffusion), and the third step is due to the diffusion of arsenate on the binding sites of the MOFs till equilibrium is reached (intraparticle diffusion starts to slow down). The rate constants of the three linear steps for each sample were calculated from the slope of the intraparticle diffusion and represented in Table S4. Interestingly, UiO-66-36TFA showed the highest values for the three rates assuring the high arsenate uptake by comparison to other MOFs. In addition to that, the first step is the fastest one of the highest rate, whereas the last step is the slowest one. Therefore, the external diffusion is the fastest step and the intraparticle diffusion is the rate-determining one.

4.5. Mechanism of the Arsenate Uptake. As mentioned in all above experiments, the arsenate uptake always followed a certain trend, and this was due to the missing linker defects that dominate the nanoscale UiO-66 MOFs modulated with monocarboxylic acids. First of all, the origin of defects must be understood, where they are compensated by a group of modulators. Theoretically, during the synthesis procedure, the linker and the modulator compete for carboxylate (CO_2^-) sites on the MOF cluster [$\text{Zr}_6(\text{OH})_4\text{O}_4(\text{CO}_2)_{12}$];⁴⁴ however, to generate missing linker defects, the modulator must deprotonate before coordinating with the MOF and must bind to at least 1 of the 12 sites on 12 different clusters that are

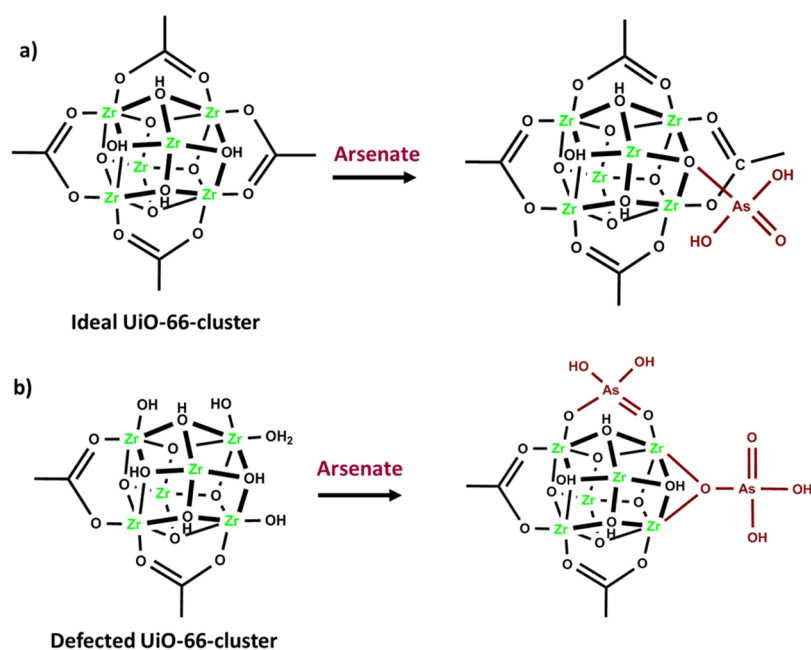


Figure 6. Possible mode of adsorption of arsenate on the ideal zirconium cluster (a) and the defected one (b).

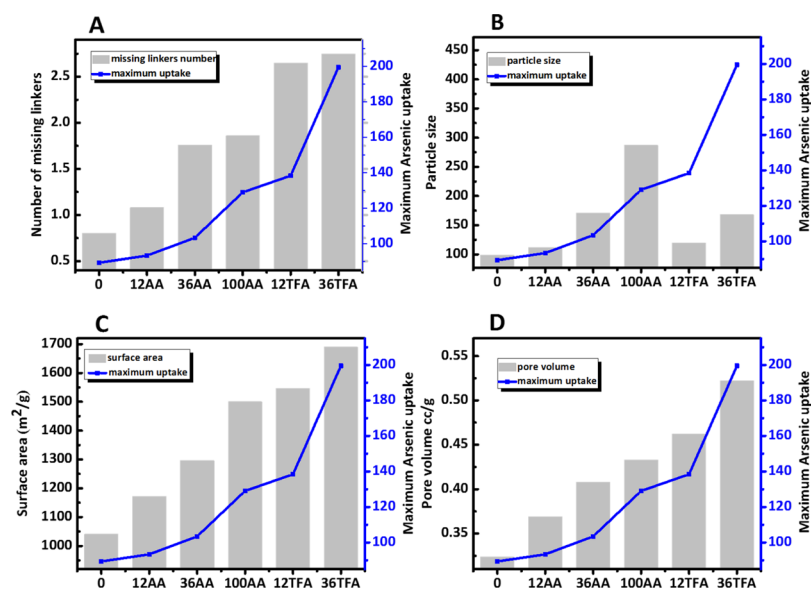


Figure 7. Effect of missing linkers (A), particle size (B), surface area (C), and pore volume (D) on the maximal arsenic uptake.

close to each other. As the ratio of the competing modulator increases, the probability of the modulator remaining linked to the cluster increases, and thus more missing linker defect can be obtained. Moreover, a more acidic modulator (lower pK_a value) has a higher deprotonation ability and thus a more defected framework.

It has been demonstrated that the first adsorption pathway for arsenate by a nondefected UiO-66 is the μ -3-O through anion exchange with the bridging hydroxyl groups on the Zr cluster, which results in the formation of four Zr–OH groups in a unit Zr₆ cluster (Figure 6).³³

However, in a highly defected UiO-66 structure, the preferred pathway for arsenate uptake by the UiO-66 structure is most likely via adsorption on the missing linker sites on the Zr₆ nodes via a singly or doubly coordination mode (Figure 6).⁶² After filling these sites, secondary binding pathways are

possible by exchanging certain BDC linkers with arsenate, leading to the formation of arsenic complexes in the MOF framework,^{33,62} and thus by increasing the defect number, more free sites become available for arsenate to bind to the Zr cluster which explain the fast and high uptake capacity of UiO-66-36TFA.

With this in mind, it is clear now why the arsenate removal increased as the defect increased whether by increasing the acid amount or the acidity of the modulator because less linker molecules were found and thus more available free sites for As (V) to attach. This is assured in Figure 7A where the arsenate uptake increases proportionally to the number of missing linkers. Figure 7B shows the change in the maximal arsenate uptake as a function of the particle size. The size follows a certain trend within the samples made with the same modulator; however, it is not the case by comparing all of

the samples with each other. In other words, it is probably that there is no strong relationship between the particle size and the adsorption capacity, indicating that the adsorption on the surface of the MOFs is not the main driving force for the process.

However, other factors could have contributed to this increase in the uptake capacity. Figure 7C,D represents the variation in the adsorption capacity compared to that of the BET surface area and pore volume, respectively, for the studied samples. Having large pore volume and having high surface area are two of the most interesting characteristics in MOFs. In theory, this means that the more the free acid sites exposed to the arsenate molecules, the higher the adsorption is. It is clear from the obtained trends that As uptake increases with surface area and pore volume of the studied samples. From these data, it could be suggested that high surface area, large pore volume, and high defect density are important parameters for the development of efficient As adsorbents.

4.6. Removal of Ultratrace (ppb) Arsenate. Because arsenate found in drinking water is found at the ppb (part per billion) level, removal of low concentration As (*V*) by the defected MOF samples was tested using the most defected MOF sample (UiO-66-36TFA) and compared to the UiO-66 sample. To this end, three batches were prepared, each of different mass of the six samples (5, 10, and 15 mg) separately added to 5 mL of 50 ppb arsenate solution. Interestingly, in all the tested tubes regardless the type and amount of adsorbent used, no arsenate was detected, meaning that more than 90% of arsenate was removed (the remaining concentration was below the detection limit of AA for arsenate). To further investigate their capacities on lower concentration level, 5 mg of each adsorbent was added to 5 ppb arsenate solution. Surprisingly, this minor mass of all the MOFs was able to eliminate all of the arsenic species in the solutions. These great results pushed us toward further investigation for the parameters of ultratrace arsenate removal, so an additional experiment using much lower masses of the adsorbents (0.01–2 mg) to remove 5 ppb concentration of arsenate was carried out. The obtained results are given in Figure S14 that shows that the uptake percentage is directly proportional to the adsorbent mass. The arsenate removal percentage increased from 80 to 100% for UiO-66-36TFA as the mass increased from 0.01 to 0.5 mg. However, 1 mg of the nonmodulated MOF was needed to accomplish 100% As removal.

This result demonstrates that UiO-66-36TFA showed not only higher elimination percentage than the nonmodulated UiO-66 but also reached the equilibrium (100% removal) at lower mass (0.5 mg) that is half the mass UiO-66 needed to reach the full adsorption (1 mg).

4.7. Postadsorption Characterizations. The used samples of UiO-66-36TFA after the adsorption were investigated by FTIR, PXRD, TGA, and SEM–EDX. Adsorption of arsenic was confirmed by FTIR, as presented in Figure S15A, where a new peak was observed at 864 cm^{-1} that is related to the combination of both symmetric and asymmetric stretching vibrations of the As–O bond. Moreover, the peak at 1020 cm^{-1} which is attributed to the vibrations of O–H groups on Zr clusters (Zr–OH) decreased in intensity in the sample after As adsorption, which means that these OH groups were engaged in the adsorption process. The PXRD patterns of the MOF after adsorption of arsenic presented in Figure S15B comply perfectly with the one before adsorption, assuring the well-retained crystallinity and high stability of the

UiO-66 MOF structure. Moreover, SEM–EDX image shown in Figure S16 reveals the presence of As on the surface of the crystals in addition. It shows the reservation of the framework morphology after the adsorption of arsenic species within the UiO-66 framework. By comparing the TGA analysis for the sample before and after adsorption found in Figure S15C, two decomposition steps that are related to the adsorption of arsenate were observed and a higher mass is left at the final stage of analysis corresponding to the remained nonvolatile arsenic oxide.

The above data show great pieces of evidence for the strong interactions between arsenate and the MOF adsorbents, which are in good agreement with kinetic and thermodynamic studies.

4.8. Anionic Coexistence Experiments. To study the practicability of the synthesized samples in real-life water treatment applications, other anionic interactions that are coexisting in water must be taken into consideration because of the ability of competing with arsenate for the sorbent adsorptive sites. Accordingly, arsenic removal experiments were conducted in the presence of the following anions separately: sodium nitrate, sodium carbonate, sodium sulfate, sodium bicarbonate, sodium chloride, sodium formate, sodium acetate, and sodium phosphate. As displayed in Figure S17, the presence of these anions did not cause any significant change in the arsenate uptake except in the case of sodium carbonate because carbonate partially dissolves the MOF framework, thus decreasing arsenic uptake.⁶⁹ This noneffective action indicated the preferable affinity for arsenate over these coexisting anionic species. However, sodium carbonate decreased the uptake to less than half that without any added anion and this could be attributed to the competition between arsenate and carbonate ions for the same available adsorption sites that are found on the surface of adsorbents.

4.9. Reusability Test. Investigating the reusability of the studied sorbent is of crucial importance; in particular, UiO-66-36TFA of the greatest defect was studied. While choosing the regenerant, certain properties must be taken into consideration including the efficiency of their desorbing capacity, keeping the adsorbent surface nondamaged, and cost effectiveness. The best regenerant tested was methanol. After collecting the postadsorbing MOF samples, they were soaked in fresh methanol for 12 h several times to desorb arsenate from the MOF material before being dried out well in the vacuum oven for the following run. The adsorption test was repeated four more times where in each cycle, the same adsorption capacity was attained without any decrease in uptake amount, as shown in Figure 8. The mass of the adsorbent after the fifth cycle was found to be 29.12 mg.

Therefore, UiO-66-36TFA can be used as a potential recyclable adsorbent for arsenate elimination.

5. CONCLUSIONS

To summarize, zirconium-based MOF nanoparticles with adjusted defects have been successfully synthesized and fully characterized. Their ability to remove arsenic from water was evaluated and discussed according to the structural features of the synthesized MOFs. After studying the sample properties and performing the adsorption experiments, it was concluded that UiO-66-36TFA, which was the most defected sample, showed the highest arsenate adsorption (200 mg g^{-1}) not only among its competitors but also among all previously reported arsenate adsorbents. In addition, the enormous performance of

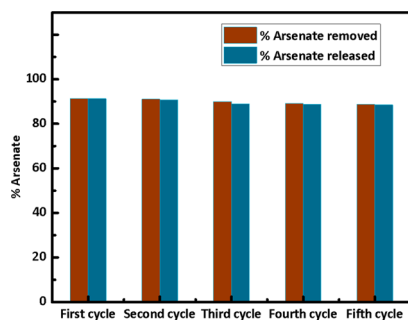


Figure 8. Removal of As from water after regeneration of UiO-66-36TFA for five cycles. $C_0 = 150 \text{ mg L}^{-1}$, $V = 10 \text{ mL}$, $m = 30 \text{ mg}$.

these nanoscale adsorbents in real water samples demonstrated their feasibility for practical applications. Examining their phenomenal characteristics, simple fabrication procedure, high crystallinity and chemical stability, impressive arsenate removal, fast kinetics, and perfect regeneration/recyclability made them of great potential toward being the best compelling candidate for arsenate purification from drinking water.

■ ASSOCIATED CONTENT

SI Supporting Information

The Supporting Information is available free of charge at <https://pubs.acs.org/doi/10.1021/acsnm.0c01696>.

Short-angle XRD of UiO-66-36TFA, pore size distribution, reaction conditions and textural properties, TGA curves, proton NMR, zeta potential measurement, Langmuir and Freundlich parameters and their fitting data, comparison of arsenate adsorption among prevailing adsorbents, adsorption of As at different temperatures, van't Hoff plot, parameters of As (V) adsorption kinetics, intraparticle diffusion models, effect of the mass on the removal efficiency of As solution at low concentration (5 ppb), postadsorption characterization (FT-IR, PXRD, TGA, and EDX), and ion effect on the adsorption of arsenate by UiO-66-36TFA (PDF)

■ AUTHOR INFORMATION

Corresponding Author

Mohamad Hmadeh – Department of Chemistry, Faculty of Arts and Sciences, American University of Beirut, Beirut 1107-2020, Lebanon; orcid.org/0000-0003-3027-3192; Email: mohamad.hmadeh@aub.edu.lb

Authors

Nisrine Assaad – Department of Chemistry, Faculty of Arts and Sciences, American University of Beirut, Beirut 1107-2020, Lebanon; orcid.org/0000-0002-9719-3309

Ghewa Sabeh – Department of Chemistry, Faculty of Arts and Sciences, American University of Beirut, Beirut 1107-2020, Lebanon; orcid.org/0000-0003-2849-8827

Complete contact information is available at: <https://pubs.acs.org/doi/10.1021/acsnm.0c01696>

Funding

This work was funded by the Lebanese National Council for Scientific Research (#103496 and #103487) and the Masri Institute (#103214).

Notes

The authors declare no competing financial interest.

■ ACKNOWLEDGMENTS

We gratefully acknowledge the funding provided by the American University of Beirut Research Board and the K. Shair Central Research Science Laboratory. We thank Asmaa Jrad and Ahmad Makkawi for their valuable discussions.

■ REFERENCES

- (1) Lv, S.-W.; Liu, J.-M.; Wang, Z.-H.; Ma, H.; Li, C.-Y.; Zhao, N.; Wang, S. Recent advances on porous organic frameworks for the adsorptive removal of hazardous materials. *J. Environ. Sci.* **2019**, *80*, 169–185.
- (2) Litter, M. I.; Morgada, M. E.; Bundschuh, J. Possible treatments for arsenic removal in Latin American waters for human consumption. *Environ. Pollut.* **2010**, *158*, 1105–1118.
- (3) Jomova, K.; Jenisova, Z.; Feszterova, M.; Baros, S.; Liska, J.; Hudecova, D.; Rhodes, C.; Valko, M. Arsenic: toxicity, oxidative stress and human disease. *J. Appl. Toxicol.* **2011**, *31*, 95–107.
- (4) Edition, F. *Guidelines for Drinking-Water Quality*; WHO Chronicle, 2011; Vol. 38, pp 104–108.
- (5) Jun, J. W.; Tong, M.; Jung, B. K.; Hasan, Z.; Zhong, C.; Jhung, S. H. Effect of central metal ions of analogous metal–organic frameworks on adsorption of organoarsenic compounds from water: plausible mechanism of adsorption and water purification. *Chem.—Eur. J.* **2015**, *21*, 347–354.
- (6) Carlin, D. J.; Naujokas, M. F.; Bradham, K. D.; Cowden, J.; Heacock, M.; Henry, H. F.; Lee, J. S.; Thomas, D. J.; Thompson, C.; Tokar, E. J. Arsenic and environmental health: state of the science and future research opportunities. *Environ. Health Perspect.* **2016**, *124*, 890–899.
- (7) Mohan, D.; Pittman, C. U., Jr. Arsenic removal from water/wastewater using adsorbents—a critical review. *J. Hazard. Mater.* **2007**, *142*, 1–53.
- (8) Huang, N.; Zhai, L.; Xu, H.; Jiang, D. Stable covalent organic frameworks for exceptional mercury removal from aqueous solutions. *J. Am. Chem. Soc.* **2017**, *139*, 2428–2434.
- (9) Yuan, Y.; Yang, Y.; Ma, X.; Meng, Q.; Wang, L.; Zhao, S.; Zhu, G. Molecularly imprinted porous aromatic frameworks and their composite components for selective extraction of uranium ions. *Adv. Mater.* **2018**, *30*, 1706507.
- (10) Sun, Q.; Aguila, B.; Earl, L. D.; Abney, C. W.; Wojtas, L.; Thallapally, P. K.; Ma, S. Covalent organic frameworks as a decorating platform for utilization and affinity enhancement of chelating sites for radionuclide sequestration. *Adv. Mater.* **2018**, *30*, 1705479.
- (11) Li, Y.; Yang, Z.; Wang, Y.; Bai, Z.; Zheng, T.; Dai, X.; Liu, S.; Gui, D.; Liu, W.; Chen, M.; Chen, L.; Diwu, J.; Zhu, L.; Zhou, R.; Chai, Z.; Albrecht-Schmitt, T. E.; Wang, S. A mesoporous cationic thorium-organic framework that rapidly traps anionic persistent organic pollutants. *Nat. Commun.* **2017**, *8*, 1354.
- (12) Wang, Y.; Liu, Z.; Li, Y.; Bai, Z.; Liu, W.; Wang, Y.; Xu, X.; Xiao, C.; Sheng, D.; Diwu, J.; Su, J.; Chai, Z.; Albrecht-Schmitt, T. E.; Wang, S. Umbellate Distortions of the Uranyl Coordination Environment Result in a Stable and Porous Polycatenated Framework That Can Effectively Remove Cesium from Aqueous Solutions. *J. Am. Chem. Soc.* **2015**, *137*, 6144–6147.
- (13) Singh, T. S.; Pant, K. K. Equilibrium, kinetics and thermodynamic studies for adsorption of As(III) on activated alumina. *Sep. Purif. Technol.* **2004**, *36*, 139–147.
- (14) Jang, M.; Chen, W.; Cannon, F. S. Preloading Hydrous Ferric Oxide into Granular Activated Carbon for Arsenic Removal. *Environ. Sci. Technol.* **2008**, *42*, 3369–3374.
- (15) Baig, S. A.; Sheng, T.; Zhu, J.; Xu, X. Performance of an Integrated Treatment System for Clean Drinking Water Production. *Clean: Soil, Air, Water* **2015**, *43*, 1450–1454.
- (16) Dobrowolski, R.; Otto, M. Preparation and evaluation of Ni-loaded activated carbon for enrichment of arsenic for analytical and environmental purposes. *Microporous Mesoporous Mater.* **2013**, *179*, 1–9.

- (17) Arstad, B.; Fjellvåg, H.; Kongshaug, K. O.; Swang, O.; Blom, R. Amine functionalised metal organic frameworks (MOFs) as adsorbents for carbon dioxide. *Adsorption* **2008**, *14*, 755–762.
- (18) Zhou, H.-C.; Long, J. R.; Yaghi, O. M. Introduction to Metal–Organic Frameworks. *Chem. Rev.* **2012**, *112*, 673–674.
- (19) Trickett, C. A.; Helal, A.; Al-Maythaly, B. A.; Yamani, Z. H.; Cordova, K. E.; Yaghi, O. M. The chemistry of metal–organic frameworks for CO₂ capture, regeneration and conversion. *Nat. Rev. Mater.* **2017**, *2*, 17045.
- (20) Hmadeh, M.; Lu, Z.; Liu, Z.; Gándara, F.; Furukawa, H.; Wan, S.; Augustyn, V.; Chang, R.; Liao, L.; Zhou, F. New porous crystals of extended metal-catecholates. *Chem. Mater.* **2012**, *24*, 3511–3513.
- (21) Katz, M. J.; Brown, Z. J.; Colón, Y. J.; Siu, P. W.; Scheidt, K. A.; Snurr, R. Q.; Hupp, J. T.; Farha, O. K. A facile synthesis of UiO-66, UiO-67 and their derivatives. *Chem. Commun.* **2013**, *49*, 9449–9451.
- (22) Liu, B.; Vellingiri, K.; Jo, S.-H.; Kumar, P.; Ok, Y. S.; Kim, K.-H. Recent advances in controlled modification of the size and morphology of metal-organic frameworks. *Nano Res.* **2018**, *11*, 4441–4467.
- (23) Furukawa, H.; Cordova, K. E.; O’Keeffe, M.; Yaghi, O. M. The chemistry and applications of metal-organic frameworks. *Science* **2013**, *341*, 1230444.
- (24) Hasan, Z.; Jhung, S. H. Removal of hazardous organics from water using metal-organic frameworks (MOFs): plausible mechanisms for selective adsorptions. *J. Hazard. Mater.* **2015**, *283*, 329–339.
- (25) Joseph, L.; Jun, B.-M.; Jang, M.; Park, C. M.; Muñoz-Senmache, J. C.; Hernández-Maldonado, A. J.; Heyden, A.; Yu, M.; Yoon, Y. Removal of contaminants of emerging concern by metal-organic framework nanoadsorbents: A review. *Chem. Eng. J.* **2019**, *369*, 928–946.
- (26) Moussa, Z.; Hmadeh, M.; Abiad, M. G.; Dib, O. H.; Patra, D. Encapsulation of curcumin in cyclodextrin-metal organic frameworks: Dissociation of loaded CD-MOFs enhances stability of curcumin. *Food Chem.* **2016**, *212*, 485–494.
- (27) Mortada, B.; Matar, T. A.; Sakaya, A.; Atallah, H.; Kara Ali, Z.; Karam, P.; Hmadeh, M. Postmetalated Zirconium Metal Organic Frameworks as a Highly Potent Bactericide. *Inorg. Chem.* **2017**, *56*, 4739–4744.
- (28) Burtch, N. C.; Jasuja, H.; Walton, K. S. Water stability and adsorption in metal–organic frameworks. *Chem. Rev.* **2014**, *114*, 10575–10612.
- (29) Jian, M.; Liu, B.; Zhang, G.; Liu, R.; Zhang, X. Adsorptive removal of arsenic from aqueous solution by zeolitic imidazolate framework-8 (ZIF-8) nanoparticles. *Colloids Surf., A* **2015**, *465*, 67–76.
- (30) Atallah, H.; ELcheikh Mahmoud, M.; Jelle, A.; Lough, A.; Hmadeh, M. A highly stable indium based metal organic framework for efficient arsenic removal from water. *Dalton Trans.* **2018**, *47*, 799–806.
- (31) Abu Tarboush, B. J.; Chouman, A.; Jonderian, A.; Ahmad, M.; Hmadeh, M.; Al-Ghoul, M. Metal–Organic Framework-74 for Ultratrace Arsenic Removal from Water: Experimental and Density Functional Theory Studies. *ACS Appl. Nano Mater.* **2018**, *1*, 3283–3292.
- (32) VuChouman, T. A.; Le, G. H.; Dao, C. D.; Dang, L. Q.; Nguyen, K. T.; Nguyen, Q. K.; Dang, P. T.; Tran, H. T. K.; Duong, Q. T.; Nguyen, T. V. Arsenic removal from aqueous solutions by adsorption using novel MIL-53 (Fe) as a highly efficient adsorbent. *RSC Adv.* **2015**, *5*, 5261–5268.
- (33) Wang, C.; Liu, X.; Chen, J. P.; Li, K. Superior removal of arsenic from water with zirconium metal-organic framework UiO-66. *Sci. Rep.* **2015**, *5*, 16613.
- (34) Yee, K.-K.; Reimer, N.; Liu, J.; Cheng, S.-Y.; Yiu, S.-M.; Weber, J.; Stock, N.; Xu, Z. Effective Mercury Sorption by Thiol-Laced Metal–Organic Frameworks: in Strong Acid and the Vapor Phase. *J. Am. Chem. Soc.* **2013**, *135*, 7795–7798.
- (35) Canivet, J.; Vandichel, M.; Farrusseng, D. Origin of highly active metal–organic framework catalysts: defects? Defects! *Dalton Trans.* **2016**, *45*, 4090–4099.
- (36) Taddei, M. When defects turn into virtues: The curious case of zirconium-based metal-organic frameworks. *Coord. Chem. Rev.* **2017**, *343*, 1–24.
- (37) Bueken, B.; Reinsch, H.; Reimer, N.; Stassen, I.; Vermoortele, F.; Ameloot, R.; Stock, N.; Kirschhock, C. E. A.; De Vos, D. A zirconium squarate metal–organic framework with modulator-dependent molecular sieving properties. *Chem. Commun.* **2014**, *50*, 10055–10058.
- (38) Vandichel, M.; Hajek, J.; Vermoortele, F.; Waroquier, M.; De Vos, D. E.; Van Speybroeck, V. Active site engineering in UiO-66 type metal–organic frameworks by intentional creation of defects: a theoretical rationalization. *CrystEngComm* **2015**, *17*, 395–406.
- (39) Gutov, O. V.; Hevia, M. G.; Escudero-Adán, E. C.; Shafir, A. Metal–Organic Framework (MOF) Defects under Control: Insights into the Missing Linker Sites and Their Implication in the Reactivity of Zirconium-Based Frameworks. *Inorg. Chem.* **2015**, *54*, 8396–8400.
- (40) Shearer, G. C.; Chavan, S.; Ethiraj, J.; Vitillo, J. G.; Svelle, S.; Olsbye, U.; Lamberti, C.; Bordiga, S.; Lillerud, K. P. Tuned to perfection: Ironing out the defects in metal–organic framework uiO-66. *Chem. Mater.* **2014**, *26*, 4068–4071.
- (41) Hu, Z.; Faucher, S.; Zhuo, Y.; Sun, Y.; Wang, S.; Zhao, D. Combination of Optimization and Metalated-Ligand Exchange: An Effective Approach to Functionalize UiO-66(Zr) MOFs for CO₂ Separation. *Chem.—Eur. J.* **2015**, *21*, 17246–17255.
- (42) Cliffe, M. J.; Hill, J. A.; Murray, C. A.; Coudert, F.-X.; Goodwin, A. L. Defect-dependent colossal negative thermal expansion in UiO-66(Hf) metal–organic framework. *Phys. Chem. Chem. Phys.* **2015**, *17*, 11586–11592.
- (43) Wu, H.; Chua, Y. S.; Krungleviciute, V.; Tyagi, M.; Chen, P.; Yildirim, T.; Zhou, W. Unusual and highly tunable missing-linker defects in zirconium metal–organic framework UiO-66 and their important effects on gas adsorption. *J. Am. Chem. Soc.* **2013**, *135*, 10525–10532.
- (44) Shearer, G. C.; Chavan, S.; Bordiga, S.; Svelle, S.; Olsbye, U.; Lillerud, K. P. Defect Engineering: Tuning the Porosity and Composition of the Metal–Organic Framework UiO-66 via Modulated Synthesis. *Chem. Mater.* **2016**, *28*, 3749–3761.
- (45) Cirujano, F. G.; Corma, A.; Llabrés i Xamena, F. X. Conversion of levulinic acid into chemicals: Synthesis of biomass derived levulinate esters over Zr-containing MOFs. *Chem. Eng. Sci.* **2015**, *124*, 52–60.
- (46) Vermoortele, F.; Bueken, B.; Le Bars, G.; Van de Voorde, B.; Vandichel, M.; Houthoofd, K.; Vimont, A.; Daturi, M.; Waroquier, M.; Van Speybroeck, V.; Kirschhock, C.; De Vos, D. E. Synthesis modulation as a tool to increase the catalytic activity of metal–organic frameworks: the unique case of UiO-66 (Zr). *J. Am. Chem. Soc.* **2013**, *135*, 11465–11468.
- (47) Cliffe, M. J.; Wan, W.; Zou, X.; Chater, P. A.; Kleppe, A. K.; Tucker, M. G.; Wilhelm, H.; Funnell, N. P.; Coudert, F.-X.; Goodwin, A. L. Correlated defect nanoregions in a metal–organic framework. *Nat. Commun.* **2014**, *5*, 4176.
- (48) Feng, D.; Wang, K.; Su, J.; Liu, T.-F.; Park, J.; Wei, Z.; Bosch, M.; Yakovenko, A.; Zou, X.; Zhou, H.-C. A Highly Stable Zeotype Mesoporous Zirconium Metal–Organic Framework with Ultralarge Pores. *Angew. Chem.* **2015**, *127*, 151–156.
- (49) Cavka, J. H.; Jakobsen, S.; Olsbye, U.; Guillou, N.; Lamberti, C.; Bordiga, S.; Lillerud, K. P. A New Zirconium Inorganic Building Brick Forming Metal Organic Frameworks with Exceptional Stability. *J. Am. Chem. Soc.* **2008**, *130*, 13850–13851.
- (50) Jrad, A.; Abu Tarboush, B. J.; Hmadeh, M.; Ahmad, M. Tuning acidity in zirconium-based metal organic frameworks catalysts for enhanced production of butyl butyrate. *Appl. Catal., A* **2019**, *570*, 31–41.
- (51) Valvekens, P.; Vermoortele, F.; De Vos, D. Metal–organic frameworks as catalysts: the role of metal active sites. *Catal. Sci. Technol.* **2013**, *3*, 1435–1445.
- (52) Audu, C. O.; Nguyen, H. G. T.; Chang, C.-Y.; Katz, M. J.; Mao, L.; Farha, O. K.; Hupp, J. T.; Nguyen, S. T. The dual capture of As V and As III by UiO-66 and analogues. *Chem. Sci.* **2016**, *7*, 6492–6498.

(53) Li, J.; Liu, Y.; Wang, X.; Zhao, G.; Ai, Y.; Han, B.; Wen, T.; Hayat, T.; Alsaedi, A.; Wang, X. Experimental and theoretical study on selenate uptake to zirconium metal–organic frameworks: Effect of defects and ligands. *Chem. Eng. J.* **2017**, *330*, 1012–1021.

(54) Howarth, A. J.; Katz, M. J.; Wang, T. C.; Platero-Prats, A. E.; Chapman, K. W.; Hupp, J. T.; Farha, O. K. High efficiency adsorption and removal of selenate and selenite from water using metal–organic frameworks. *J. Am. Chem. Soc.* **2015**, *137*, 7488–7494.

(55) Gu, Y.; Xie, D.; Ma, Y.; Qin, W.; Zhang, H.; Wang, G.; Zhang, Y.; Zhao, H. Size modulation of zirconium-based metal organic frameworks for highly efficient phosphate remediation. *ACS Appl. Mater. Interfaces* **2017**, *9*, 32151–32160.

(56) Li, J.; Liu, Y.; Ai, Y.; Alsaedi, A.; Hayat, T.; Wang, X. Combined experimental and theoretical investigation on selective removal of mercury ions by metal organic frameworks modified with thiol groups. *Chem. Eng. J.* **2018**, *354*, 790–801.

(57) Liang, W.; Coghlan, C. J.; Ragon, F.; Rubio-Martinez, M.; D'Alessandro, D. M.; Babarao, R. Defect engineering of UiO-66 for CO₂ and H₂O uptake—a combined experimental and simulation study. *Dalton Trans.* **2016**, *45*, 4496–4500.

(58) Wang, K.; Li, C.; Liang, Y.; Han, T.; Huang, H.; Yang, Q.; Liu, D.; Zhong, C. Rational construction of defects in a metal–organic framework for highly efficient adsorption and separation of dyes. *Chem. Eng. J.* **2016**, *289*, 486–493.

(59) Chen, Z.; Wang, X.; Noh, H.; Ayoub, G.; Peterson, G. W.; Buru, C. T.; Islamoglu, T.; Farha, O. K. Scalable, room temperature, and water-based synthesis of functionalized zirconium-based metal–organic frameworks for toxic chemical removal. *CrystEngComm* **2019**, *21*, 2409–2415.

(60) Shan, B.; McIntyre, S. M.; Armstrong, M. R.; Shen, Y.; Mu, B. Investigation of Missing-Cluster Defects in UiO-66 and Ferrocene Deposition into Defect-Induced Cavities. *Ind. Eng. Chem. Res.* **2018**, *57*, 14233–14241.

(61) Valenzano, L.; Civaleri, B.; Chavan, S.; Bordiga, S.; Nilsen, M. H.; Jakobsen, S.; Lillerud, K. P.; Lamberti, C. Disclosing the complex structure of UiO-66 metal organic framework: a synergic combination of experiment and theory. *Chem. Mater.* **2011**, *23*, 1700–1718.

(62) Molavi, H.; Eskandari, A.; Shojaei, A.; Mousavi, S. A. Enhancing CO₂/N₂ adsorption selectivity via post-synthetic modification of NH₂-UiO-66 (Zr). *Microporous Mesoporous Mater.* **2018**, *257*, 193–201.

(63) Van de Voorde, B.; Stassen, I.; Bueken, B.; Vermoortele, F.; De Vos, D.; Ameloot, R.; Tan, J.-C.; Bennett, T. D. Improving the mechanical stability of zirconium-based metal–organic frameworks by incorporation of acidic modulators. *J. Mater. Chem. A* **2015**, *3*, 1737–1742.

(64) Sekar, M.; Sakthi, V.; Rengaraj, S. Kinetics and equilibrium adsorption study of lead (II) onto activated carbon prepared from coconut shell. *J. Colloid Interface Sci.* **2004**, *279*, 307–313.

(65) Xiong, Y. Y.; Li, J. Q.; Gong, L. L.; Feng, X. F.; Meng, L. N.; Zhang, L.; Meng, P. P.; Luo, M. B.; Luo, F. Using MOF-74 for Hg²⁺ removal from ultra-low concentration aqueous solution. *J. Solid State Chem.* **2017**, *246*, 16–22.

(66) Li, L.; Ma, W.; Shen, S.; Huang, H.; Bai, Y.; Liu, H. A combined experimental and theoretical study on the extraction of uranium by amino-derived Metal–Organic Frameworks through Post-Synthetic Strategy. *ACS Appl. Mater. Interfaces* **2016**, *8*, 31032–31041.

(67) Al-Anber, M. A. *Thermodynamics Approach in the Adsorption of Heavy Metals*; INTECH Open Access Publisher, 2011.

(68) Srihari, V.; Das, A. The kinetic and thermodynamic studies of phenol-sorption onto three agro-based carbons. *Desalination* **2008**, *225*, 220–234.

(69) Chu, J.; Ke, F.-S.; Wang, Y.; Feng, X.; Chen, W.; Ai, X.; Yang, H.; Cao, Y. Facile and reversible digestion and regeneration of zirconium-based metal-organic frameworks. *Commun. Chem.* **2020**, *3*, 5.